An SIT-BJT Operation Model for SITh in the Blocking State

Yang Jianhong†, Wang Zaixing, and Li Siyuan

(*Institute of Microelectronics, School of Physical Science and Technology, Lanzhou University, Lanzhou 730000, China*)

Abstract: A SIT-BJT model is proposed for static induction thyristors (SITh) operation in the blocking state. On the basis of the physical mechanism, this model is presented analytically in terms of governing equations that link the electrical parameters to the structural parameters. The model is verified by numerical simulation and theoretical analysis. Based on the model, the variations of the electrical parameters such as the potential barrier, the anode junction voltage drop, and the current amplification factor are studied and discussed.

Key words: static induction thyristor; SIT-BJT model; current amplification factor
PACC: 7360J **EEACC**: 2550X; 2560B
CLC number: TN385 **Document code**: A **Article ID**: 0253-4177(2008)04-0645-05

1 Introduction

SITh is a power switch device capable of high current and high voltage[1~6]. Most works discuss the fabrication process, measurement of *I-V* characteristics, and the anode current performance. However, few works are devoted to the gate and the cathode currents, and few models for SITh working in the blocking-state have been reported. Therefore, a practical physical model to describe the operating mechanism of SITh is required.

A silicon-based surface-gate normally-off SITh is chosen as the device prototype in this work. This device is easier to fabricate than buried-gate devices[7] and is capable of avoiding the latch-up effects during the switching process more easily than its normally-on counterpart. In addition, the gate-cathode is negatively biased to exploit the blocking capabilities.

A new model in terms of governing equations showing the main ideas is presented. The model is verified extensively by numerical simulation and theoretical analysis. The simulated values agree well with the experimental results. The variations of the electrical parameters of SITh are examined in view of device physics, aiming to give insights into the model.

2 SIT-BJT model for SITh operating in blocking state

Figure 1 schematically shows the structural diagram of a unit in SITh. When the device operates in the forward blocking state, the holes are injected into the drift region from the anode, and are collected by the gate. Meanwhile, the electrons inject into the drift region from the cathode, which are controlled by the channel barrier, and are combined with the holes in the drift region. Thus, this structure can be regarded as a combination of two parts: a SIT part, which includes the n^+-cathode region, the p^+-gate region, the n^--channel region, and the n^--base region and a BJT part, which includes the p^+-anode region, the n^--base region, and the p^+-gate region. In the BJT, the p^+-anode region and the p^+-gate region act as the emitter and the collector, respectively (assuming the gate-base junction is reverse biased). The n^--base region and the p^+-gate (collector) region are common to both the SIT and the BJT, i.e., there are mutual effects between the SIT and the BJT. Thus, a SITh can be represented by the "SIT-BJT model" shown in Fig. 2. Furthermore, as there is a similar operation mechanism in the buried-gate SITh, the "SIT-BJT model"

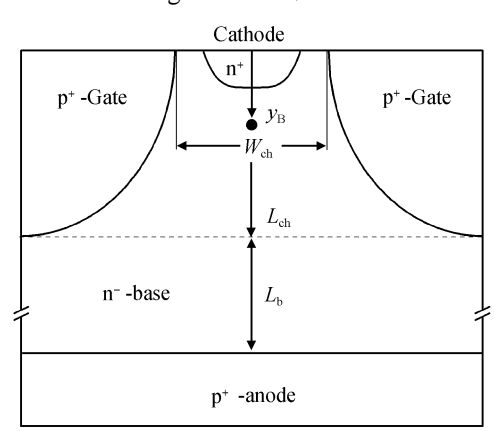

Fig. 1 Structural diagram of a unit in SITh, where y_B is the location of the "saddle point" of the potential barrier, L_{ch} is the channel length, W_{ch} is the minimum physical width of the channel, and L_b is the thickness of the base region

† Corresponding author. Email: zaixin02@st.lzu.edu.cn
Received 14 October 2007, revised manuscript received 30 November 2007

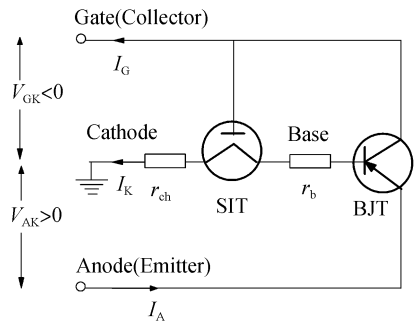

Fig. 2 Conceptual diagram of the SIT-BJT model for SITh operation in the blocking state The base region is shared by the SIT and the BJT.

can also describe its mechanism.

In this model, the cathode current I_K from the cathode in the SIT part provides the base current for the BJT. On the other hand, the holes injected from the anode (emitter) junction are collected by the gate (collector), constituting the gate current I_G. The total current, I_A, is the sum of the cathode current I_K and the gate current I_G:

$$I_A = I_K + I_G = (1 + \beta_{BJT}) I_K \tag{1}$$

where

$$I_G = \beta_{BJT} I_K \tag{2}$$

and β_{BJT} is the current amplification factor of the BJT.

The key factor limiting the cathode current (I_K) is the height of the barrier ($\phi_{B\text{-}SIT}$) in the channel[8,9]:

$$I_K = I_{K0} \exp\left(-\frac{q\phi_{B\text{-}SIT}}{kT}\right) \tag{3}$$

where I_{K0} is nearly a constant and the other symbols have their conventional meanings. On the other hand, the key factors limiting the gate current (I_G) are β_{BJT} and $V_{J\text{-}BJT}$. Here, $V_{J\text{-}BJT}$ is the forward voltage drop in the anode-base junction:

$$I_G = \alpha_{BJT} I_A = \frac{\beta_{BJT}}{1 + \beta_{BJT}} I_A = \frac{\beta_{BJT}}{1 + \beta_{BJT}} I_{A0} \exp\left(\frac{qV_{J\text{-}BJT}}{nkT}\right) \tag{4}$$

where $\alpha_{BJT} = \beta_{BJT}/(1 + \beta_{BJT})$ represents the base current transfer ratio of the BJT, I_{A0} is nearly constant, and n is the ideality factor depending the injection level.

All the parameters, e.g., $\phi_{B\text{-}SIT}$, $V_{J\text{-}BJT}$, β_{BJT}, and n, vary with the device operating conditions. In particular, both the potential barrier ($\phi_{B\text{-}SIT}$) and the junction voltage ($V_{J\text{-}BJT}$) float with, but are not directly dependent on, the applied voltages (V_{GK} and V_{AK}). This differentiates SITh from many other devices. Another important feature of SITh is that $\phi_{B\text{-}SIT}$ and $V_{J\text{-}BJT}$ have an interdependent relationship, such that the SIT and BJT can accommodate each other. This feature becomes clearer if we insert Eqs. (3) and (4) into Eq. (2), yielding:

$$I_{K0} \exp\left(-\frac{q\phi_{B\text{-}SIT}}{kT}\right) = \frac{I_{A0}}{1 + \beta_{BJT}} \exp\left(\frac{qV_{J\text{-}BJT}}{nkT}\right) \tag{5}$$

Table 1 Structural parameters of the SITh under investigation

Parameter	Symbol	Value
Surface doping of the Anode	N_A	$1\times10^{19}\,cm^{-3}$
Surface doping of the Gate	N_G	$5\times10^{18}\,cm^{-3}$
Surface doping of the Cathode	N_K	$1\times10^{19}\,cm^{-3}$
Doping of the Base	N_B	$5\times10^{13}\,cm^{-3}$
Pitch depth	D	$15\mu m$
Anode junction depth	D_A	$40\mu m$
Gate junction depth	D_G	$7\mu m$
Cathode junction depth	D_K	$1\mu m$
Pitch width	W	$15\mu m$
Window width of the Gate	W_G	$1\mu m$
Window width of the Cathode	W_K	$1\mu m$

The left- and right-hand sides concern the SIT and BJT, respectively. This equation reveals the mutual effects and interplay between the SIT and the BJT. Obviously, $\phi_{B\text{-}SIT}$ and $V_{J\text{-}BJT}$ cannot vary independently. Moreover, this equation relates the two active parts by various parameters such as structural parameters and electrical parameters. Thus, the operation of the SITh in the blocking state is governed by Eq. (5).

3 Analysis and discussion

This section is intended to examine the above model by means of numerical simulation and theoretical analysis. We performed 2D simulations on device properties. For the purpose of comparison, we used the same geometric and doping parameters in all simulations. The device under investigation is a normally-off device, i.e., the channel is already pinched off at zero bias and a potential barrier is built in the channel[10,11]. The gate- and anode-cathode biasing voltages (V_{GK} and V_{AK}) are set to be negative and positive, respectively, to examine the blocking capabilities. The doping and structural parameters of the device are given in Table 1.

3.1 Verification of the SIT-BJT model

Focusing on the governing equation for the blocking state, equation (5) can be rewritten in the following form:

$$\left(\phi_{B\text{-}SIT} + \frac{V_{J\text{-}BJT}}{n}\right) - \frac{kT}{q}\ln(1 + \beta_{BJT}) = \frac{kT}{q}\ln\left(\frac{I_{K0}}{I_{A0}}\right) \tag{6}$$

where all the electrical parameters are on the left-hand side, and all the characteristic parameters are on the right-hand side. Figure 3 shows the numerical results of the variations of the potential barrier ($\phi_{B\text{-}SIT}$) and the junction voltage ($V_{J\text{-}BJT}$), where the gate bias is fixed at $V_{GK} = -2\,V$. $\phi_{B\text{-}SIT}$ and $V_{J\text{-}BJT}$ vary in inverse directions with the applied anode bias (V_{AK}): $V_{J\text{-}BJT}$ increases while $\phi_{B\text{-}SIT}$ decreases. This manifests the interplay between the SIT and BJT. Thus, the increasing anode bias exerts influence on the electric field in the

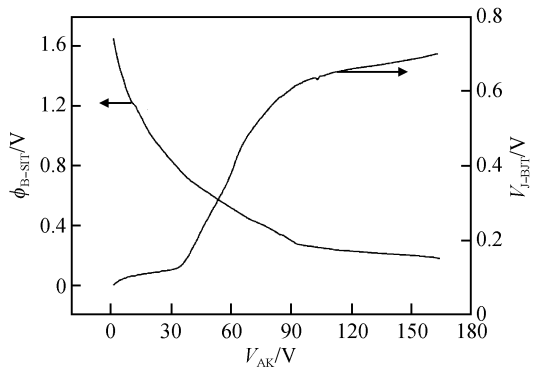

Fig. 3　Variations of potential barrier ($\phi_{B\text{-}SIT}$) and junction voltage ($V_{J\text{-}BJT}$) with the applied bias (V_{AK}) in the blocking state

vicinity of the gate region (including the channel region), resulting in the lowering of $\phi_{B\text{-}SIT}$. In turn, the increased base current (I_K) due to the lowering of $\phi_{B\text{-}SIT}$ is amplified by the BJT, and the anode (emitter) junction must increase the injection level, resulting in the increase of $V_{J\text{-}BJT}$. This is in accordance with the idea of the SIT-BJT model.

A special region of V_{AK} = 0～30V exists where the potential barrier is sufficiently high and the junction voltage is sufficiently low such that neither of them can allow notable currents in the device. As seen from the *I-V* characteristics in Fig. 6, the currents in this region are negligibly small due to the thermal generation of carriers in the space charge region of the gate junction. In other words, the reciprocity of SIT and BJT is not activated in this region and the device operates in a "dead region" because the currents are limited by the thermal generation. In the other vast range of V_{AK}, the reciprocity of SIT and BJT is present until the device is switched into the conducting state. As demonstrated below, the width of the "dead region" is responsible for the magnitude of the breakover voltage.

The variations of the current amplification factor (β_{BJT}) are shown in Fig. 4, from which we have removed the meaningless data in the "dead region". β_{BJT} changes dramatically with the varying operating conditions. Beyond the "dead region", β_{BJT} increases due to the raised injection level of the BJT when the device is driven into the recombination-dominated regime. β_{BJT} increases to a maximum when the device is driven into the injection-dominated regime in which the role of BJT is enhanced. β_{BJT} decreases, however, when the high-level injection effect becomes dominant. These variations are also depicted in the *I-V* characteristics (Fig. 6(a)). Interestingly, at all breakover voltages, β_{BJT} drops to approximately 1 regardless of the varying gate biases.

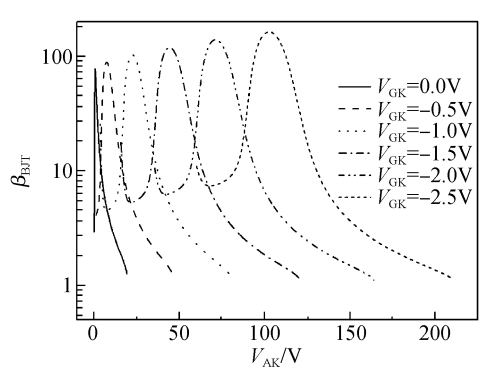

Fig. 4　Variations of the current amplification factor of the BJT (β_{BJT}) with applied biases (V_{GK} and V_{AK})　The lines denote the variations in the forward blocking state.

All the above variations of $\phi_{B\text{-}SIT}$, $V_{J\text{-}BJT}$, and β_{BJT} are, however, under the restriction of Eq. (6). To show this, we examine the equality of Eq. (6) by letting

$$\frac{kT}{q}\ln\left(\frac{I_{K0}}{I_{A0}}\right)=\frac{kT}{q}\ln\left(\frac{W_{eff}}{W}\times\frac{D_n}{D_p}\times\frac{L'_b}{y_B}\times\frac{N_K N_B}{n_i^2}\right)\equiv C_1 \tag{7a}$$

and

$$\left(\phi_{B\text{-}SIT}+\frac{V_{J\text{-}BJT}}{n}\right)-\frac{kT}{q}\ln(1+\beta_{BJT})\equiv C_2 \tag{7b}$$

where I_{K0} and I_{A0} are[10,12]:

$$I_{K0}=qA_{eff}N_K\frac{D_n}{y_B} \tag{8a}$$

$$I_{A0}\approx qA_A\frac{D_p}{L_p}\times\frac{n_i^2}{N_B}\mathrm{ctnh}\left(\frac{L'_b}{L_p}\right)\approx qA_A\frac{D_p}{L'_p}\times\frac{n_i^2}{N_B} \tag{8b}$$

respectively, in which

$$L'_b=L_b-\left[\frac{2\varepsilon(V_{AK\text{-}BO}-V_{GK})}{q(m+1)N_B}\right]^{\frac{1}{2}} \tag{9}$$

represents the quasi-neutral base thickness, A_{eff} denotes the effective area of the channel in the SIT part, A_A denotes the anode junction area in the BJT part, W_{eff} is the effective width of the channel, y_B is the location of the peak of the potential barrier (the "saddle point"[13] measured from the top surface), and D_n and D_p are the diffusion coefficients of electrons and holes, respectively. m is a magnification factor accounting for the increasing space charges due to movable holes in the gate junction; i. e., the space charge density should be $q(m+1)N_B$ rather than qN_B when in the high-level injection regime. The meanings of the other symbols are indicated in Table 1. Thus, by checking whether $C_1 = C_2$, the equality of Eq. (10), and hence, the validity of the SIT-BJT model, can be examined.

Figure 5 shows the comparison between the calculated C_1 and simulated C_2. In this figure, C_1 is calculated using Eq. (7a) and C_2 is simulated using Eq. (7b) (i. e., using the data of $\phi_{B\text{-}SIT}$, $V_{J\text{-}BJT}$, and β_{BJT} in Figs. 3 and 4, but the meaningless data in the "dead

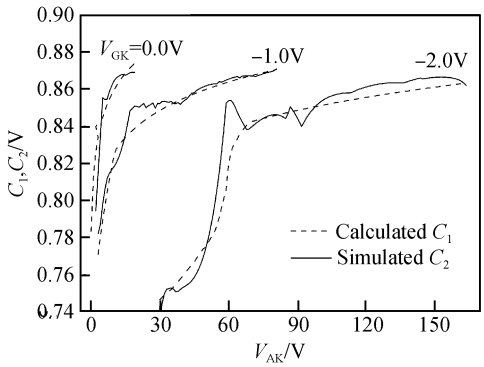

Fig. 5 Comparisons between the calculated C_1 and the simulated C_2 to examine the equality of Eq. (6) In calculating C_1, the location of the "saddle point" (y_B) is assumed to decrease only in the recombination-dominated regime by moving from the center of the channel ($y_B = 4.5\mu$m) to the cathode edge of the channel ($y_B = 1.0\mu$m); The effective channel width (W_{eff}) is assumed to increase only in the injection-dominated regime from one-fifth of the channel physical width ($W_{eff} = W_{ch}/5 = 0.64\mu$m) to four-fifths of that ($W_{eff} = 4W_{ch}/5 = 2.56\mu$m). The quasi-neutral base thickness (L'_b) is calculated using Eq. (9), in which the magnification factor (m) is assumed to increase notably only in the injection-dominated regime from 0 to 2 synchronously with the increasing anode bias (V_{AK}) until breakover occurs.

region" have been removed). The ideality factor, n, is assumed to vary from 2 to 1 when the device is driven from the recombination-dominated regime to the injection-dominated regime. Figure 5 indicates that C_1 and C_2 have the same varying pattern. C_1 is variable because the effective channel width (W_{eff}) becomes larger when more of the channel region is occupied by carriers due to the raised injection level. Meanwhile, the location of the "saddle point" of the potential barrier (y_B) also becomes smaller due to its movement in the channel (closer to the cathode), and, the thickness of the quasi-neutral base (L'_b) becomes smaller at higher biases as well. Consequently, C_1 is smaller in the lower bias range than in the higher bias range due to the increase in $(kT/q)\ln(W_{eff}L'_b/y_B)$. Moreover, both the calculated C_1 and the simulated C_2 are in good agreement and the average difference between them is less than 1%, well within the tolerance of numerical accuracy. This means that the equality of Eq. (6) is retained regardless of the varying biasing voltages and parameters. Therefore, the SIT-BJT model is reliable for the SITh operation in the blocking state.

3.2 Analysis of *I-V* characteristics

Figure 6 shows the *I-V* characteristics of the SITh. In the blocking state (Fig. 6(a)), the mutual effects are evident (beyond the "dead region"): $I_G > I_K$ as can be explained by the SIT-BJT model with $I_G = \beta_{BJT} I_K$ and $\beta_{BJT} > 1$. In the large current region[14], although I_G is still larger than I_K, the increase rate of I_G is smaller than that of I_K, as a result of the increase in the Gummel number of the base, as can be inferred from Fig. 7.

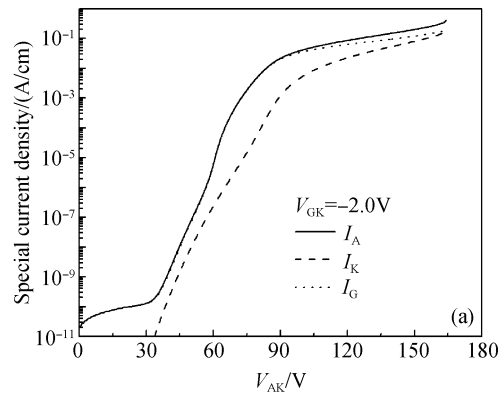

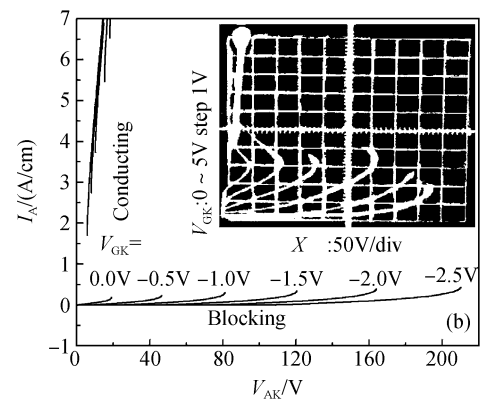

Fig. 6 *I-V* characteristics of the SITh (a) In the blocking state at fixed gate bias $V_{GK} = -2$V (in semilog scale); (b) Full range *I-V* curves at varying gate bias (in linear scale), where there is an inserted experimental *I-V* result for purpose of comparison (the device structures in both simulation and experiment are the same).

4 Conclusion

The operation of static induction thyristors has

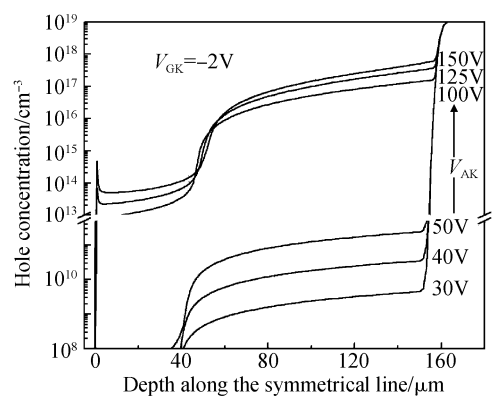

Fig. 7 Distribution of hole concentration along the device symmetrical line: variations with the anode bias (V_{AK})

been studied both qualitatively and quantitatively based on a newly-proposed model. The model is presented in terms of governing equations. We conclude that the operations of static induction thyristors in the forward blocking state are subjected to the reciprocity between the parasitic SIT and BJT. The model is in good agreement with simulation results and is capable of interpreting the *I-V* characteristics conveniently. Furthermore, the implications of the model are helpful in device design, fabrication, and application.

References

[1] Tang Ying, Liu Su, Li Siyuan, et al. A novel structure for a static induction transistor. Chinese Journal of Semiconductors, 2007, 28(6): 918(in Chinese) [唐颖, 刘肃, 李思渊, 等. 一种新型结构的静电感应晶体管. 半导体学报, 2006, 28(6): 918]

[2] Tang Ying, Liu Su, Li Siyuan, et al. Study on combined channel parameters of a static induction transistor. Semiconductor Science and Technology, 2007, 22(7): 806

[3] Wang Yongshun, Li Siyuan, Hu Dongqing. A microwave high power static induction transistor with double dielectrics gate structure. Chinese Journal of Semiconductors, 2004, 25(1): 19

[4] Nishizawa J, Muraoka K, Tamamushi T, et al. Low-loss high-speed switching devices, 2300-V 150-A static induction thyristor. IEEE Trans Electron Devices, 1978, 32(4): 822

[5] Hu Dongqing, Li Siyuan, Wang Yongshun. Analysis on characteristics of static induction transistor using mirror method. Chinese Journal of Semiconductors, 2005, 26(2): 258

[6] Wessels B W, Baliga B J. Vertical channel field-controlled thyristors with high gain and fast switching speeds. IEEE Trans Electron Devices, 1978, 25(10): 1261

[7] Jiang Yanfeng, Huang Qing'an. Simulation of SiC anisotropic etching using cellular automata method. Chinese Journal of Semiconductors, 2005, 26(3): 618 (in Chinese) [姜岩峰, 黄庆安. 硅各向异性腐蚀的原子级模拟. 半导体学报, 2005, 26(3): 618]

[8] Nishizawa J, Terasaki T, Shibata J. Field effect transistor versus analog transistor. IEEE Trans Electron Devices, 1975, 22(4): 185

[9] Mentzner D, Schröder D. A SITh-model for CAE in power electronics. Proc Int Symp Power Semiconductor Device IC's, 1990: 204

[10] Nakamura Y, Tadano H, Sugiyama S, et al. Normally-off high speed SI-thyristor. Electron Devices Meeting, 1982, 28: 480

[11] Ohmi T. Punching through device and its integration-static induction transistor. IEEE Trans Electron Devices, 1980, 27(3): 536

[12] Streetman B G, Banerjee S. Solid state electronic devices. 5th ed. New Jersey: Prentice Hall, 2000

[13] Baliga B J. Barrier-controlled current conduction in field-controlled thyristors. Solid State Electron, 1981, 24(7): 617

[14] Yang Jianhong. Electrically-induced dipole domain in the junction-barrier structure under the high-level injection condition. Semiconductor Science and Technology, 2003, 18(6): L31

静电感应晶闸管在阻断态时的 SIT-BJT 等效工作模型

杨建红†　汪再兴　李思渊

（兰州大学物理科学与技术学院微电子研究所，兰州　730000）

摘要： 提出了一种描述静电感应晶闸管在阻断态时的工作机理的 SIT-BJT 等效模型. 在器件物理的基础上，分析得到的这个模型衔接了静电感应晶闸管的物理参数和结构参数，而且给出的数值分析和理论分析证明了这个模型的正确性. 在该模型的基础上，讨论了势垒、阳极结的电势降落和电流的放大因子等电参数的变化.

关键词： 静电感应晶闸管；SIT-BJT 等效模型；电流放大因子

PACC： 7360J　　**EEACC：** 2550X；2560B

中图分类号： TN385　　**文献标识码：** A　　**文章编号：** 0253-4177(2008)04-0645-05

† 通信作者. Email: zaixin02@st.lzu.edu.cn

2007-10-14 收到，2007-11-30 定稿